






Titanium Oxynitriding by Plasma-Assisted Thermochemical Treatments Using a Competitive Atmosphere of H_2 - N_2 - O_2

J. O. Vitoriano^a , R. S. Pessoa^b , A. A. Mendes Filho^c , J. Amorim Filho^b ,
C. Alves-Junior^{a,b,*} 

^aUniversidade Federal do Rio Grande do Norte, Departamento de Engenharia Mecânica, Natal, 59078-970, Natal, RN, Brasil.

^bInstituto Tecnológico de Aeronáutica, Departamento de Ciência e Tecnologia Aeroespacial, Laboratório de Plasmas e Processos, 12228-900, São José dos Campos, SP, Brasil.

^cUniversidade Federal do ABC, Centro de Engenharia, Modelagem e Ciências Sociais Aplicadas, 09210580, Santo André, SP, Brasil.

Received: June 13, 2023; Revised: September 17, 2023; Accepted: October 20, 2023

The incorporation of oxygen and/or nitrogen into the titanium lattice has garnered significant attention due to the broad spectrum of intermediate properties that can be achieved between TiN and TiO₂. This article delves into the investigation of surface modification of titanium through plasma-assisted thermochemical treatments employing H₂-N₂-O₂ mixtures. The flow rate of the reducing gas (H₂) remained constant at 24 sccm, while the flow rates of N₂ and O₂ were adjusted to yield a total flow rate of 60 sccm. Analysis using GIXRD, Raman spectroscopy, and XPS demonstrated that TiN exhibits stability exclusively in an oxygen-free atmosphere, while TiO₂, in contrast, necessitates an oxygen flux equal to or exceeding 18 sccm for stability. Furthermore, it was found that the presence of nitrogen in the plasma atmosphere resulted in a greater expansion of the α -titanium lattice, although the solubility of interstitials decreased. These findings highlight the potential for a controlled approach to producing solid solutions or titanium oxynitrides.

Keywords: Plasma, Thermochemical treatment; Plasma diagnostic; GIXRD; Titanium oxynitride.

1. Introduction

Ti-based alloys are significant in various applications, including biomedical ones, due to their excellent strength-to-weight ratio, superior corrosion resistance, notable thermal and electrical conductivity, and biocompatibility, among other properties¹⁻³. Furthermore, these properties are highly dependent on the composition of the alloys, particularly nitrogen and/or oxygen gases, the main constituents of the atmosphere-air⁴⁻⁷.

A comprehensive understanding of how titanium absorbs nitrogen and oxygen is crucial in devising strategies for the creation of nitrides, oxides, oxynitrides, or related phases. These phases can exhibit intriguing properties suitable for various applications. Literature increasingly suggests the possibility of various stoichiometries and oxidation states, ranging from the solid solution of these interstitials in the α -titanium lattice, α -Ti(N,O) to TiO₂, or TiN, or a solid cubic solution (NaCl-type) from titanium (III) nitride (TiN), to the cubic titanium (II) oxide (TiO). These are collectively referred to as oxynitrides TiN_xO_{1-x}⁸⁻¹⁴.

Although numerous experimental and theoretical studies exist for α -Ti(N,O) solid solutions, TiN_xO_{1-x} solid cubic solution (NaCl-type), TiO₂, and TiN compounds and

the conditions for their formation^{8,9,12,13,15-17}, there is still a degree of uncertainty regarding the bonding and structure of TiN_xO_{1-x}. Various experimental methods have been employed to synthesize and understand the formation mechanism of TiO_xN_y¹⁸⁻²².

The plasma-assisted thermochemical technique is conducted in the abnormal glow discharge region. Here, a uniform, stable glow, separated from the cathode (workpiece) by the cathode sheath, produces a current density that is directly proportional to the voltage drop, making it easily controllable^{23,24}. Different events can happen during the plasma-surface interaction. Ions are accelerated within the cathode sheath, bombarding the sample surface. Atoms dislodged from the surface due to sputtering interact with plasma species, forming unstable compounds. These compounds then redeposit and recombine on the sample's surface, releasing atoms that diffuse into the titanium^{25,26}. If the energy required for compound formation surpasses the collision energy, compounds might form and either remain on the surface or return to the plasma. The oxidation of titanium, which occurs when oxygen ions or molecules collide with the titanium surface, exemplifies the former scenario. The latter is represented by the reduction of TiO₂ by hydrogen ions, molecules, or atoms.

*e-mail: alvesclodomirol@gmail.com

In multi-element plasma atmospheres, numerous concurrent events might transpire during treatment. These events can include precipitation, adsorption, sputtering, reduction, oxidation, and species diffusion on the surface²⁷⁻³⁰.

In this study, both nitriding and oxidation processes were undertaken simultaneously, facilitated by an H₂-reducing atmosphere. A continuous H₂ atmosphere flow was used to inhibit the spontaneous formation of native oxide. As a result, the plasma active species would consistently meet a titanium surface devoid of native oxides. This oxide-free state was ensured by introducing a sufficient hydrogen flow prior to treatment until the O-I peak (777 nm), as observed in optical emission spectroscopy (OES) of the residual gas plasma, disappeared³¹. By controlling the nitriding/oxidation environment and adjusting the N₂/O₂ ratio while using hydrogen to remove native oxides, we aim to provide a comprehensive understanding of the Ti-N-O system.

2. Materials and Methods

2.1. Samples preparation

Commercially pure grade 2 titanium discs, measuring 1.0 mm in thickness and 16.0 mm in diameter, were used for the plasma-assisted thermochemical experiments. The discs were metallographically prepared as detailed in previous publication³¹. After polishing, they were cleaned three times in an ultrasonic bath containing enzymatic detergent, 70% ethanol, and distilled water. The samples were immersed for 10 minutes in each cleaning bath to remove any contaminants (hardened oils, dirt, grease, fingerprints, etc.) that might interfere with the plasma-assisted surface modification process.

2.2. Plasma-assisted thermochemical process

Plasma treatments were conducted using a DC plasma apparatus, as detailed in³¹. After placing the sample in the sample holder, the reactor was sealed and pumped down to a residual pressure of 2.7 Pa. Subsequently, a hydrogen gas flow of 24 sccm was introduced. The O-I (777 nm) peak, denoted by spectroscopic notation O-I (3p⁴ 4s² 3P0 → 3P1), was monitored via optical emission spectroscopy (OES) until its disappearance, which occurred at 49.3 Pa. The samples

underwent a pre-treatment at 900 V and 120°C for a duration of 30 minutes (a typical cleaning condition utilized in our laboratory) to cleanse the samples, particularly to eliminate impurities and oxide films from the titanium surface. For plasma treatment, a pressure of 200 Pa was employed, ensuring an abnormal discharge regime where the voltage varies linearly with the current. Different H₂ + N₂ + O₂ mixtures were used, maintaining a constant total flow (60 sccm) and hydrogen flow (24 sccm), as outlined in Table 1.

To ensure uniformity in temperature across all experimental conditions, adjustments were made to both the voltage and current. Following this, either nitrogen, oxygen, or a combination of both gases was introduced until the system stabilized at a pressure of 200 Pa. The temperature during the process was consistently maintained at 400°C, with each treatment lasting for a duration of 1 h (as detailed in Table 1). Continuous monitoring of the plasma was achieved using optical emission spectroscopy. Specifically, the Ocean Optics USB 4000 spectrometer was employed, which operates over a wavelength range of 180.2 nm to 897.1 nm. This device boasts a 3648-element CCD array, ensuring high-resolution spectral data with an optical resolution of approximately 0.3 nm (FWHM). Wavelength calibration was meticulously performed on the USB4000 spectrometer using a mercury-argon calibration light source to guarantee accuracy in spectral readings. In addition to this, fiber optics from Ocean Optics (QP 1000-2-UV-BX) were utilized to enhance the precision of data acquisition.

2.3. Material characterization

After the plasma treatment, both the crystallography and chemical composition of the samples were assessed. Crystallographic characterization was conducted via X-ray diffraction (XRD) using a SHIMADZU® XRD-6000 (with a copper target tube, λ = 1.54060 nm, 30 mA, and 40 kV). In-depth layer analyses were carried out using the GIXRD technique (Seeman-Bohlin geometry), integrated with a thin layer analysis accessory (THA-1101) for low-angle incidence. For Grazing Incidence X-ray Diffraction (GIXRD), incidence angles of 0.5, 1.0, and 15.0 degrees were utilized. The associated X-ray information depth ranges were determined based on the mass attenuation coefficient of pure titanium, calculated using the Beer-Lambert law (HighScore Plus).

Table 1. Experimental conditions employed in this study. Samples are denoted as $Ti-H_O^N$, where the superscript indicates the nitrogen flux and the subscript indicates the oxygen flux.

Samples	Flux (sccm)			Temperature (°C)	Time (h)	Pressure (Torr)
	H ₂	N ₂	O ₂			
Ti	-	-	-	-	-	-
Ti-H ₃₆ ⁰	24	0	36	400	1	200
Ti-H ₂₇ ⁹	24	9	27	400	1	200
Ti-H ₁₈ ¹⁸	24	18	18	400	1	200
Ti-H ₉ ²⁷	24	27	9	400	1	200
Ti-H ₀ ³⁶	24	36	0	400	1	200

These depths were approximately 0.09 μm , 0.181–0.189 μm , and 0.71 – 2.08 μm , respectively. For this calculation, the titanium density was considered as 4.51 g/cm^3 , and the mass absorption coefficient of Cu K-alpha radiation was taken as 202.4 cm^2/g . An angular range from 20° to 60° (2 θ) was scanned at a speed of 0.02°/s.

Raman scattering measurements were performed using a T64000 Horiba Jobin-Yvon triple Raman spectrometer, equipped with a CCD detector 1024x256 – OPEN-3LD/R. The excitation was provided by a Verdi G5 Laser (Coherent Inc.) operating at 532 nm (green) with a power of 1 mW focused on a 100 \times objective (resulting in a laser spot diameter of 1 μm). Acquisition parameters were set to 10 acquisitions, an exposure time of 5 s, and a confocal aperture of 6.5 μm . XPS spectra were captured using a Thermo Fisher Scientific K-Alpha+ spectrometer with a monochromatic Al K- α X-ray source (Waltham, MA, USA). The energy scale was calibrated referencing the adventitious C 1s peak at 284.8 eV. High-resolution spectra from the Ti 2p, N 1s, and O 1s regions were gathered to evaluate the surface chemical states. Broad Raman spectra of the treated samples were analyzed by deconvoluting the peaks into four individual Gaussian peaks. Both quantitative and qualitative analyses of XPS and Raman spectra, for standard and treated samples, were executed using the OriginPro 2018 64-bit software^{32,33}.

3. Results and Discussion

3.1. Plasma diagnostics during titanium plasma treatment

In examining the OES spectra (Figure 1) for all treatment conditions, intensity variations of the active species were

evident upon adding oxygen to the treatment atmosphere. Notable changes were observed, primarily for O (777 nm), O (844 nm), H_α (656.5 nm), H_β (486.1 nm), as well as the second positive and first negative band systems of nitrogen.

A closer examination of the wavelength region between 306 nm and 315 nm reveals that the deconvoluted peaks of the OH band (306.8 nm, 309.4 nm), from the system $A^2\Sigma-X^2\Pi$, also increase with the introduction of more oxygen flux. Both O_2 and H_2O can efficiently repair oxygen vacancy defects through their dissociation. The dissociation of O_2 at the oxygen vacancies of $TiO_2(110)$ can heal these defects, returning the surface to its stoichiometric state. Conversely, the dissociation of H_2O results in the formation of two OH groups on the surface. These OH groups can substantially alter the electronic properties of $TiO_2(110)$, potentially leading to additional adsorption, diffusion, and dissociation of O_2 and H_2O ¹⁹.

The strength of O_2 adsorption is also notably influenced by the extent of oxygen coverage. The energy required for O_2 adsorption decreases significantly as the unit cell's size expands. This phenomenon can be ascribed to the binding mechanism, which is intrinsically tied to the capture of electrons linked to the vacancy. As vacancy coverage increases, the configuration favoring dissociation becomes more energetically favorable, facilitating more straightforward O_2 dissociation³⁴.

3.2. Surface color analysis

The surfaces of the samples post-oxynitriding did not exhibit notable microstructural differences. However, a color variation was observed, dependent on the composition of the treatment atmosphere (Figure 2).

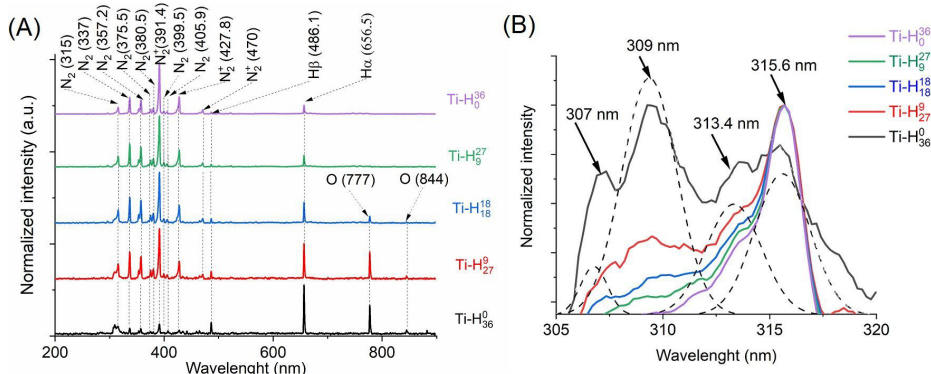


Figure 1. OES spectra from plasmas produced under varying experimental conditions utilized in this study (A), with detailed views of OH peaks between 306 nm and 315 nm (B).

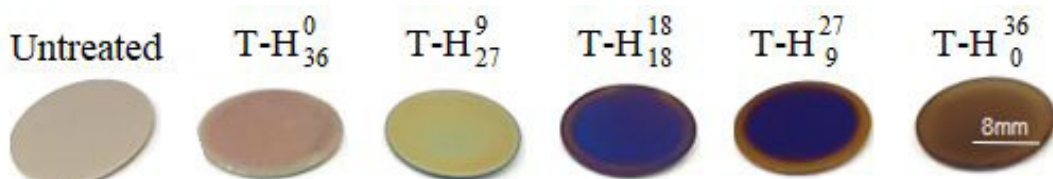


Figure 2. Color variation on the sample surfaces for different plasma treatment atmospheres.

Using the RGB color space, the untreated sample was identified as light gray (#E3E3DB). The oxidized sample exhibited a combination of light gray and pink hues (#E5D2CA). Samples subjected to nitriding displayed light brown and pink colors (#D39473). The colors of other surfaces varied from light blue (#9787A3) to dark blue (#5443BB) as the oxygen flow ranged from 27 sccm to 9 sccm. Clear rings, approximately 1 mm in thickness, were observed along the edges of the samples. These rings, referred to as restriction rings, are caused by distortions in the electric field within the edge region³⁵. Several studies have indicated that δ -TiN nitride possesses a golden hue due to its high nitrogen content. However, certain oxynitride coatings display a violet or grayish-violet shade. Clearly, these color variations are linked to the concentration gradients present in the Ti-N-O system^{36,37}.

3.3. GIXRD characterization

Structural changes dependent on the composition of the atmosphere were observed. The GIXRD patterns, using a grazing incidence angle of 1° (Figure 3A), show differences when oxygen is replaced by nitrogen in the plasma atmosphere. For comparison, we referenced the XRD pattern database: face-centered cubic TiN structure (ICDD card 00-087-0629), α -Ti hexagonal structure (ICDD card 01-089-2762), and TiO_2 tetragonal structure (ICDD card 01-076-1941). For the untreated sample, in addition to the reflections of (100), (002), (101), and (102) from polycrystalline α -Ti, the reflection (101) of native TiO_2 was also observed.

The disappearance of this peak in other samples suggests that the pretreatment process effectively removed the native TiO_2 . In plasma treatments using oxygen-rich atmospheres, namely $\text{Ti}-\text{H}_{36}^0$, $\text{Ti}-\text{H}_{27}^9$, and $\text{Ti}-\text{H}_{18}^{18}$, the intensity of the TiO_2 peaks correlates with the oxygen flow. For plasma treatment in an atmosphere devoid of oxygen, peaks identified as TiN (200) are evident. A closer examination of the diffractograms reveals that the reflections of α -Ti planes (102), (101), (002), and (100) in plasma-treated samples are broader and shifted to the left compared to the untreated sample. Reflections from the Ti plane (002) (Figure 3B) display a more pronounced shift to the left for the treated samples, suggesting a solid solution whose interplanar distance increases when interstitials are introduced. For the $\text{Ti}-\text{H}_{36}^0$ sample, beyond the leftward deviation, an asymmetry of the peak is evident, suggesting the presence of two convoluted peaks. The first, at 37.8° degrees, can be attributed to the solid solution of α -Ti (002), and the second, at 38.8° degrees, tentatively suggests the presence of the $\text{TiO}_{0.3}$ structure (ICDD card 00-073-1581) under this condition. This hypothesis gains further support when analyzing reflections from the Ti (101) (Figure 3C) and Ti (102) planes (Figure 3D).

The peak of the $\text{Ti}-\text{H}_{36}^0$ sample exhibits a more pronounced shift to the left compared to the other samples, hinting at the presence of the $\text{TiO}_{0.3}$ peak alongside the α -Ti(O) peak of the solid solution. Figures 3C and 3D also reveal peaks associated with the TiO_2 phase.

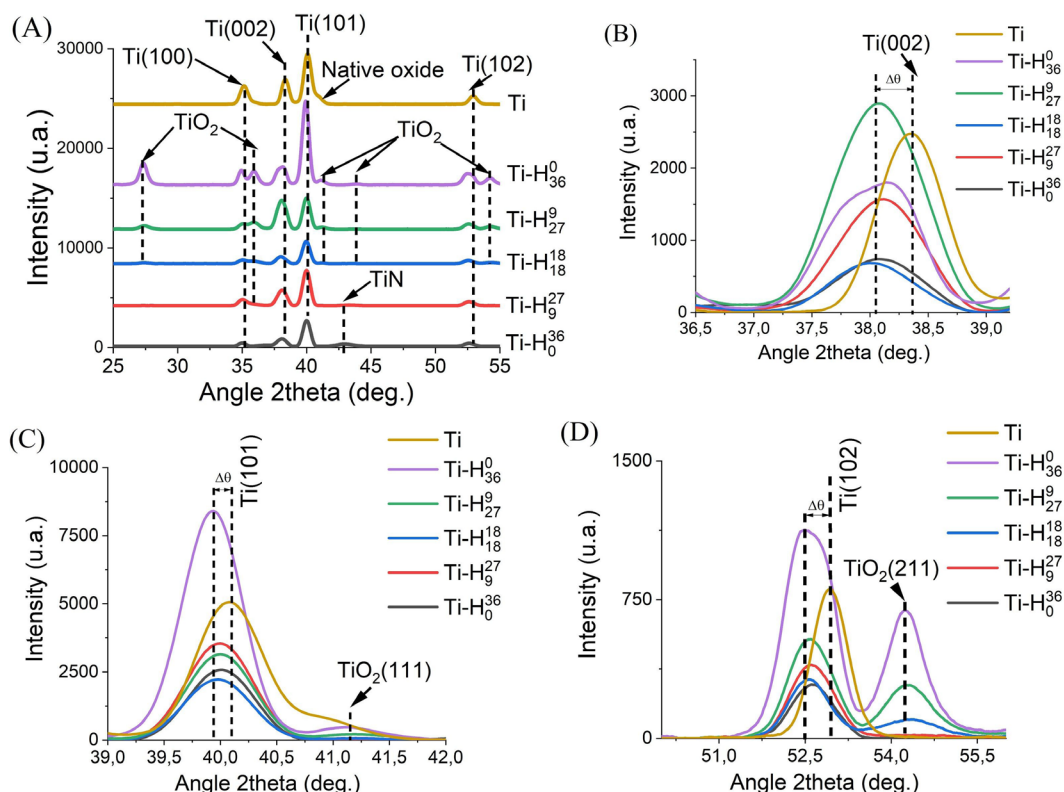


Figure 3. (A) GIXRD patterns of oxynitrided titanium surfaces, taken at an incidence angle of 1° ; (B-D) Detail of peak shifts for the solid solution corresponding to Ti (002), Ti (101), and Ti (102) planes, respectively.

The parameters “a” and “c” of the α -Ti hexagonal lattice, as determined from the reflection of the plane (100), are presented in Figure 4. These measurements align with literature findings, which show that the insertion of interstitial atoms leads to a pronounced expansion of the c-axis of the α -Ti lattice, with the a-axis being less affected. The $Ti-H_{18}^{18}$ sample exhibited the maximum values for the lattice parameters, with “c” at 4.74 Å and “a” at 2.95 Å. When only oxygen occupies the interstices of the α -Ti lattice, these values correspond to a concentration of 20% atomic oxygen. This behavior echoes literature findings emphasizing the significant expansion of the c-axis due to the incorporation of interstitial atoms, while the a-axis remains comparatively stable^{38,39}. It is noteworthy that the $Ti-H_{18}^{18}$ sample reached the aforementioned maximum values, consistent with a concentration of 20% atomic oxygen when solely oxygen is present in the α -Ti lattice interstices¹.

Given that nitrogen, with its larger atomic radius, is expected to cause more lattice expansion than oxygen, it's plausible that the interstitial concentration for the $Ti-H_{18}^{18}$ sample might be reduced¹⁴. This significant lattice expansion of α -Ti by nitrogen becomes evident when we track the substitution of oxygen by nitrogen from the $Ti-H_{36}^0$ to the $Ti-H_{18}^{18}$ condition. At elevated nitrogen concentrations, there's a noticeable decrease in the values of the “c” and “a” lattice parameters. A comparable peak has been previously identified for oxygen solutions in α -Ti at an oxygen concentration of 0.33 at. %, and this was attributed to the structured arrangement of the oxygen atoms¹⁴.

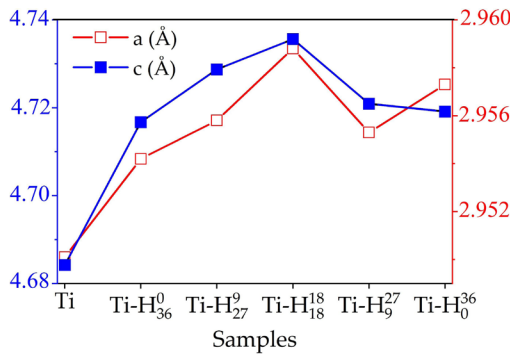


Figure 4. Variation in the lattice parameters of the α -Ti phase as a function of nitrogen and oxygen flow.

In our study, a potential ordering of nitrogen atoms, followed by the precipitation of the TiN phase, might be at play.

Interestingly, the lattice parameters — and therefore the unit cell volume — of the $Ti-H_{27}^9$ sample were found to be lower than those of the $Ti-H_{18}^{18}$ sample (Table 2). This observation appears counterintuitive, especially considering the larger atomic radius of nitrogen (0.71 Å) in comparison to oxygen (0.60 Å)^{40,41}. One potential explanation could be the diminished absorption of nitrogen by titanium in a competitive nitrogen-oxygen atmosphere.

By using various grazing incidence angles, we can qualitatively determine the thickness of the different films formed on the sample surfaces. To emphasize the diffraction peaks, we only displayed the diffractograms of the samples treated with the maximum flows of nitrogen or oxygen, in addition to the $Ti-H_{18}^{18}$ and Ti samples (see Figure 5). By considering the X-ray penetration depth for each incidence angle, which is calculated using the Beer-Lambert law, we can qualitatively assess both the diffusion depth of nitrogen and oxygen in the solid solution and the thickness of the films.

The displacement of the peaks corresponding to Ti (002), Ti (101), and Ti (102) in the oxynitrided samples vanishes when the incidence angle is adjusted to 15 degrees. Given that the X-ray information depth range, calculated using the Beer-Lambert law, lies between 0.71 and 2.08 μ m, we can conclude that the diffusion depth of interstitials is less than 2.08 μ m. In Figure 5, the sample $Ti-H_{18}^{18}$ not only exhibits a shifted peak but also displays an asymmetric shape with a shoulder, identified as the $TiO_{0.3}$ phase. This figure further reveals that the TiN phase is exclusive to the oxygen-free plasma atmosphere, while the TiO_2 phase emerges in atmospheres with an oxygen flow of 18 sccm or greater.

These insights bolster the notion that the oxynitriding treatment fosters the formation of thin films, either of TiO_2 or TiN, contingent upon the combined nitrogen and oxygen atmosphere. This is followed by the development of a solid solution of oxygen and/or nitrogen in the α -Ti. An asymmetry in the α -Ti peaks, which is not evident in other samples, is detected for the $Ti-H_{36}^0$ sample and can be ascribed to the $TiO_{0.3}$ phase.

Since this process is thermally activated and the temperature remained consistent across all experimental setups, it's logical to anticipate the same penetration depth for a given interstitial element. Minor variations in the relative intensity values might stem from the disparity in

Table 2. Lattice parameters (a and c), c/a ratio, and cell volume for oxygen and/or nitrogen solid solutions in the α -Ti lattice.

Samples	a(Å)	c(Å)	c/a	v(Å ³)
Ti	2.9501	4.6842	1.5878	35.31
$Ti-H_{36}^0$	2.9542	4.7167	1.5966	35.65
$Ti-H_{27}^9$	2.9558	4.7287	1.5998	35.78
$Ti-H_{18}^{18}$	2.9588	4.7356	1.6005	35.90
$Ti-H_9^{27}$	2.9553	4.7209	1.5974	35.71
$Ti-H_0^{36}$	2.9573	4.7191	1.5957	35.74
Ti (ICSD 43416)	2.9511	4.6843	1.5873	35.33

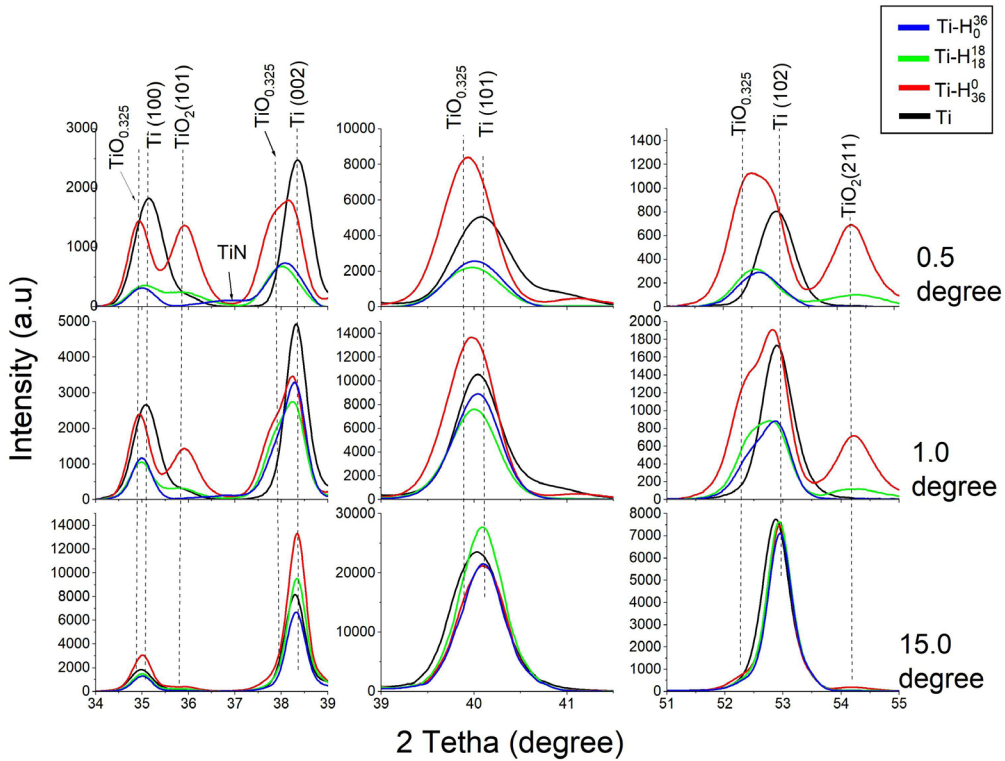


Figure 5. XRD patterns, obtained at grazing incidence angles of 0.5, 1, and 15 degrees, are presented for samples $Ti-H_0^{36}$, $Ti-H_{36}^0$, $Ti-H_{18}^{18}$, and Ti .

the diffusion coefficients for oxygen and nitrogen, which are approximately 10^{-22} m²/s and 10^{-23} m²/s, respectively⁴².

3.4. Raman spectroscopy analysis

The scattering of light in plasma-treated samples, attributed to Ti-N and Ti-O bonds, can be observed in the Raman spectra (Figure 6). By comparing the control sample with the treated ones, structural variations induced by the solid solutions in α -Ti become evident. The introduction of nitrogen and oxygen into interstitial sites alters the Raman spectrum^{32,43}.

The dispersion in the acoustic range is primarily influenced by the vibrations of the heavier titanium ions ($150\text{--}300\text{ cm}^{-1}$), while the dispersion in the optical band is influenced by vibrations of the lighter ions, such as oxygen and nitrogen ($400\text{--}650\text{ cm}^{-1}$)^{44,45}. Thus, Raman signals associated with the acoustic transverse (TA) and acoustic longitudinal (LA) vibrational modes are linked to the vibrations of the interstitial atoms. In contrast, Raman signals corresponding to the optical vibrational modes (both transverse and longitudinal) are associated with the Ti atoms.

A semi-quantitative analysis of the concentration of interstitial ions in the titanium lattice, (N, O)/Ti, can be deduced. By dividing the value of the area under the curve (To + Lo), which represents the presence of interstitials, by the area under the curve of the region (Ta+La), which indicates the presence of Ti⁴⁶⁻⁴⁸, we obtain a value proportional to the concentration (N, O)/Ti (Figure 7).

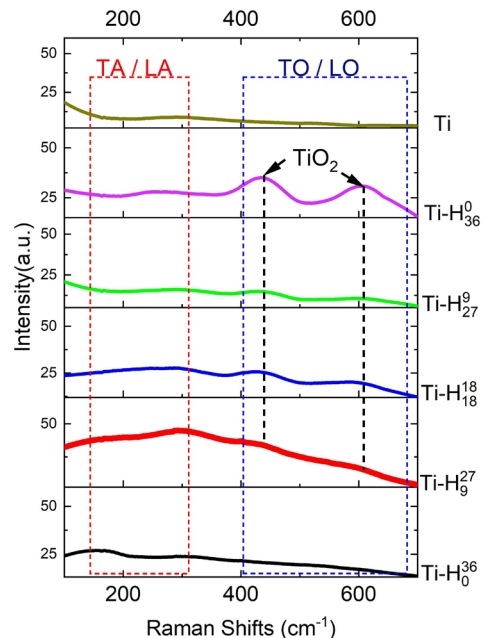


Figure 6. Raman scattering spectra of the oxynitrided titanium surface.

For the condition $Ti-H_0^{36}$, the calculated ratio $A_{T_o+L_o}/A_{T_a+L_a}$ was approximately 0.91, suggesting a TiN phase⁴⁶, consistent with the structure observed in X-ray diffraction. When

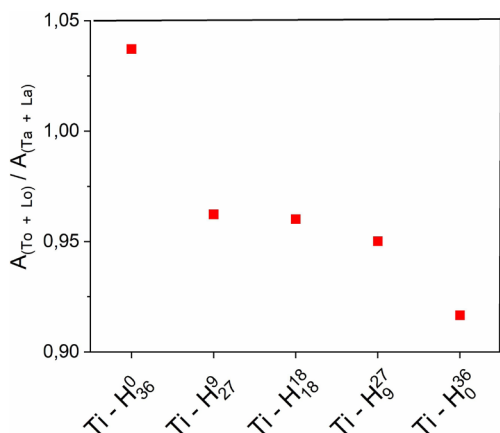


Figure 7. Ratio of the areas under the curves for the acoustic (Ta/La) and optical (To/Lo) scattering regions for the investigated samples.

nitrogen is substituted with oxygen in the plasma atmosphere, a modest and progressive increase in the $A_{T_o+L_o} / A_{T_a+L_a}$ ratio is observed. This implies that in atmospheres where nitriding and oxidation compete, there's a decrease in oxygen solubility. This hypothesis gains strength when looking at the extreme condition, $Ti-H_{36}^0$, where the atmosphere is purely oxidizing, leading to a marked increase in oxygen solubility. The substitution of nitrogen with oxygen also manifested in the emergence of Raman bands of TiO_2 (rutile) at the characteristic peaks of 430 cm^{-1} and 590 cm^{-1} ⁴⁹.

3.5. X-ray photoelectron spectroscopy

The XPS survey spectra allow for analysis of the first monolayers on the titanium surface, where the peaks of the O1s, Ti2p, C1s, and N1s spectra can be observed (Figure 8A). We have examined two areas of the XPS spectra: the Ti 2p region, ranging from 468 eV to 452 eV (Figure 8B), and the

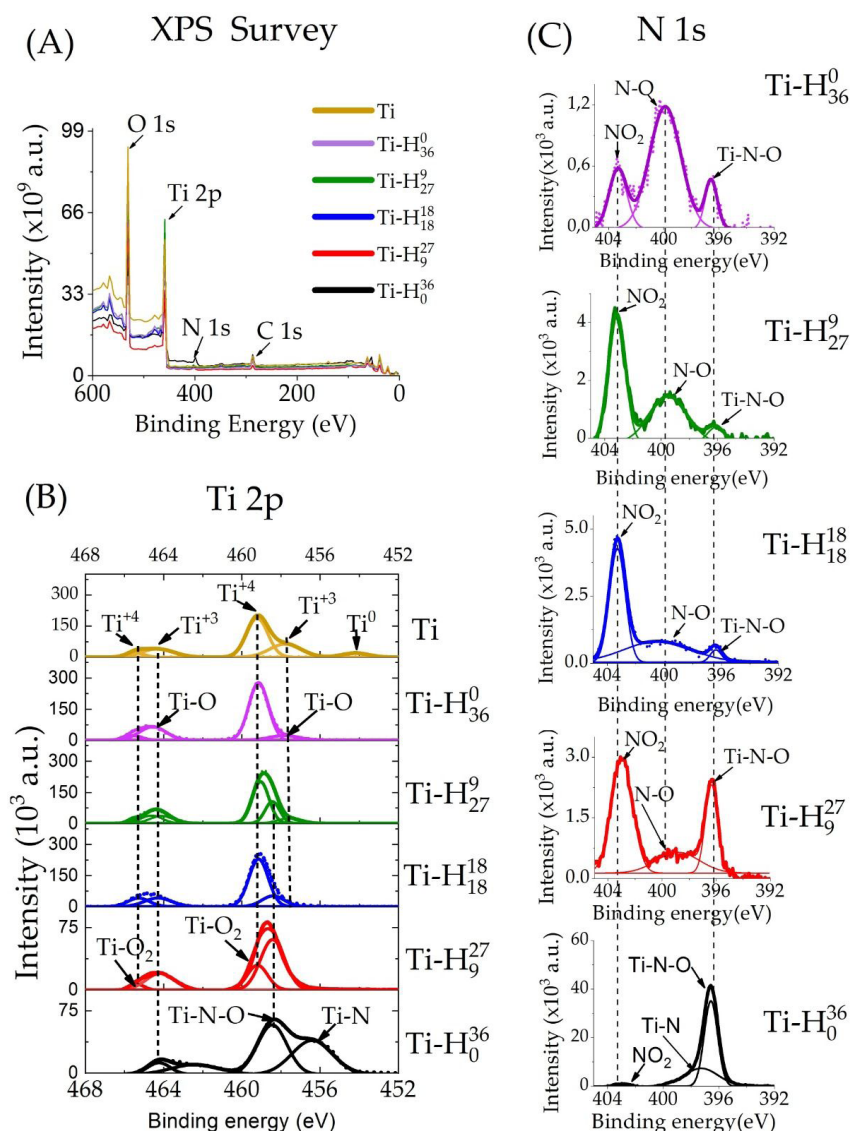


Figure 8. (A) XPS spectra obtained before and after plasma treatment under various conditions; (B) Deconvolution of the high-resolution Ti 2p spectra; and (C) High-resolution Ti N1s spectra.

N1s region, ranging from 392 eV to 406 eV (Figure 8C). The deconvoluted Ti 2p peak reveals that the untreated sample displays titanium in its Ti^0 , Ti^{3+} , and Ti^{4+} oxidation states. The Ti^0 peak corresponds to metallic titanium, while Ti^{4+} and Ti^{3+} are typically associated with the oxidation states in TiO_2 and Ti_2O_3 compounds, respectively^{17,33,50-52}, as evident in Figure 8B. In this peak, the TiN phase is visible exclusively in the sample Ti_0^{36} , where there's no O₂ in the atmosphere. When nitrogen is introduced to the atmosphere, the peak intensities of Ti-N-O decrease, supporting the hypothesis that nitrogen's presence in the atmosphere reduces the absorption of interstitials.

Turning our attention to the N1s region (Figure 8C), it's observed that for the $Ti-H_0^{36}$ sample, the most pronounced peak is centered at 396.6 eV, with a tail extending to 400 eV, hinting at a secondary phase. Upon deconvolution, one of the peaks is centered at 397.2 eV, attributed to TiN⁵³, while another peak at 396.6 eV is slightly higher than the peak in other conditions (396.4 eV) and can be linked to Ti-N-O.

Literature data identify the peak at 399.6 eV as chemisorbed nitrogen⁵⁰, and a shift to an energy of 399.8 eV corresponds to N-O bonds⁵⁴. The peak at 402.5 eV indicates N atoms being incorporated into the TiO_2 lattices. Notably, the vertical axis representing peak intensities in the N 1s spectra has a different scale depending on the N₂ concentration in the atmosphere. For the Ti_0^{36} condition, it is 15 times larger than the other conditions. Consequently, the percentage of N-O bonds is observed to increase with the rise in O₂ partial pressure.

4. Conclusion

This study explored complex phase formation dynamics on titanium surfaces during plasma-assisted thermochemical treatments in a variable atmosphere of reduction, oxidation, and nitriding. Maintaining a consistent H₂ reductant flow at 24 sccm alongside O₂ and N₂ yielded a total flow of 60 sccm. TiN exclusively formed in non-oxidizing conditions, while TiO_2 stabilized in atmospheres with 18 sccm or more of oxidizing elements, highlighting phase sensitivity. The adaptable α -Ti crystal lattice readily incorporated oxygen or nitrogen, causing lattice expansion with nitrogen substitution. While the TiN_xO_{1-x} cubic solution remained undetected, $TiO_{0.3}$ emerged as an anomaly in the $Ti-H_0^{36}$ specimen. Employing an H₂ reductant facilitated solid solution precipitation, enabling control over nitrogen and oxygen concentrations within titanium solid solutions, promising enhanced material properties.

5. Acknowledgements

This project was funded by the National Council for Scientific and Technological Development (CNPq) under grant numbers 402536/2021-5 and 304422/2021-5, as well as by the National Institute of Surface Engineering with grant number CNPq465423/2014-0.

6. References

- Liu X, Chu PK, Ding C. Surface modification of titanium, titanium alloys, and related materials for biomedical applications. *Mater Sci Eng Rep.* 2004;47(3-4):49-121. <http://dx.doi.org/10.1016/j.mser.2004.11.001>.
- Wang X, Zhao Y, Mølhave K, Sun H. Engineering the surface/interface structures of titanium dioxide micro and nano architectures towards environmental and electrochemical applications. *Nanomaterials.* 2017;7(11):382. <http://dx.doi.org/10.3390/nano7110382>.
- Straumal BB, Gornakova AS, Kilmametov AR, Rabkin E, Anisimova NY, Kiselevskiy MV. β -Ti-based alloys for medical applications. *Russ J Non-Ferrous Met.* 2021;62(1):54-63. <http://dx.doi.org/10.3103/S1067821221010156>.
- Zhecheva A, Sha W, Malinov S, Long A. Enhancing the microstructure and properties of titanium alloys through nitriding and other surface engineering methods. *Surf Coat Tech.* 2005;200(7):2192-207. <http://dx.doi.org/10.1016/j.surfcoat.2004.07.115>.
- Mucha NR, Som J, Shaji S, Fialkova S, Apte PR, Balasubramanian B, et al. Electrical and optical properties of titanium oxynitride thin films. *J Mater Sci.* 2020;55(12):5123-34. <http://dx.doi.org/10.1007/s10853-019-04278-x>.
- Graciani J, Hamad S, Sanz JF. Changing the physical and chemical properties of titanium oxynitrides $TiN_{1-x}O_x$ by changing the composition. *Phys Rev B Condens Matter Mater Phys.* 2009;80(18):184112. <http://dx.doi.org/10.1103/PhysRevB.80.184112>.
- Chen SC, Sung KY, Tzeng WY, Wu KH, Juang JY, Uen TM, et al. Microstructure and magnetic properties of oxidized titanium nitride thin films in situ grown by pulsed laser deposition. *J Phys D Appl Phys.* 2013;46(7):404-5. <http://dx.doi.org/10.1088/0022-3727/46/7/075002>.
- Sahoo S, Alpay SP, Hebert RJ. Surface phase diagrams of titanium in Oxygen, Nitrogen and Hydrogen environments: a first principles analysis. *Surf Sci.* 2018;677:18-25. <http://dx.doi.org/10.1016/j.susc.2018.05.007>.
- Jansen F, Hoffmann A, Henkel J, Rahimi K, Caumanns T, Kuehne AJC. Low-temperature synthesis of titanium oxynitride nanoparticles. *Nanomaterials.* 2021;11(4):1-9. <http://dx.doi.org/10.3390/nano11040847>.
- Khwansungnoen P, Chaiyakun S, Rattana T. Room temperature sputtered titanium oxynitride thin films: the influence of oxygen addition. *Thin Solid Films.* 2020;711:1-7. <http://dx.doi.org/10.1016/j.tsf.2020.138269>.
- Wei W, Zhao W, Liu G, Cao Z. Thermodynamic description of the Ti-C-N-O system. *Calphad.* 2023;80:1-12. <http://dx.doi.org/10.1016/j.calphad.2022.102520>.
- Yaskiv OI, Pohrel'yuk IM, Fedirko VM, Lee DB, Tkachuk OV. Formation of oxynitrides on titanium alloys by gas diffusion treatment. *Thin Solid Films.* 2011;519(19):6508-14. <http://dx.doi.org/10.1016/j.tsf.2011.04.219>.
- Vintaikin BE, Elchaninova VA, Smirnov AE, Novikov AA. Effect of preliminary erosive cutting on the thermochemical treatment of a vt6 alloy and the structure of diffusion layers. *Russ Metall.* 2020;2020(9):1008-12. <http://dx.doi.org/10.1134/S0036029520090165>.
- Kværndrup FB, Küçükylidiz ÖC, Winther G, Somers MAJ, Christiansen TL. Extreme hardening of titanium with colossal interstitial contents of nitrogen and oxygen. *Mater Sci Eng A.* 2021;813:1-10. <http://dx.doi.org/10.1016/j.msea.2021.141033>.
- Saha NC, Tompkins HG. Titanium nitride oxidation chemistry: an x-ray photoelectron spectroscopy study. *J Appl Phys.* 1992;72(7):3072-9. <http://dx.doi.org/10.1063/1.351465>.
- Yang L, Wang CZ, Lin S, Cao Y, Liu X. Early stage of oxidation on titanium surface by reactive molecular dynamics simulation [Internet]. 2018 [cited 2023 June 13]. Available from: www.techscience.com/
- Kuznetsov MV, Zhuravlev JF, Zhilyaev VA, Gubanov VA. XPS study of the nitrides, oxides and oxynitrides of titanium. *J Electron Spectrosc Relat Phenom.* 1992;58(1-2):1-9. [http://dx.doi.org/10.1016/0368-2048\(92\)80001-O](http://dx.doi.org/10.1016/0368-2048(92)80001-O).

18. Wu H, Yang D, Zhu X, Gu P, Sun H, Wangyang P, et al. Effect of the nitrogen-oxygen ratio on the position of N atoms in the TiO₂ lattice of N-doped TiO₂ thin films prepared by DC magnetron sputtering. *CrystEngComm*. 2018;20(29):4133-40. <http://dx.doi.org/10.1039/C8CE00773J>.
19. Ahmed M, Xinxin G. A review of metal oxynitrides for photocatalysis. *Inorg Chem Front*. 2016;3(5):578-90. <http://dx.doi.org/10.1039/C5QI00202H>.
20. Lin L, Xu H, Gao H, Zhu X, Hessel V. Plasma-assisted nitrogen fixation in nanomaterials: Fabrication, characterization, and application. *J Phys D Appl Phys*. 2020;53(13):1-24. <http://dx.doi.org/10.1088/1361-6463/ab5f1f>.
21. Fabreguette F, Imhoff L, Guillot J, Domenichini B, Marco de Lucas MC, Sibillot P, et al. Temperature and substrate influence on the structure of TiN_xO_y thin films grown by low pressure metal organic chemical vapour deposition. *Surf Coat Tech*. 2000;125(1-3):396-9. [http://dx.doi.org/10.1016/S0257-8972\(99\)00588-5](http://dx.doi.org/10.1016/S0257-8972(99)00588-5).
22. Braz DC, Barbosa JCP, Nunes A Fo, Rocha RCS, Silva DR, Alves C Jr. Influence of plasma species on the surface properties modification of titanium treated with a N₂-Ar-O₂ plasma. *Materia*. 2012;17:1035-44. <http://dx.doi.org/10.1590/S1517-70762012000200009>.
23. Kapczynski MP, Gil C, Kinast EJ, Santos CA. Surface modification of titanium by plasma nitriding. *Mater Res*. 2003;6(2):265-71. <http://dx.doi.org/10.1590/S1516-14392003000200023>.
24. Ribeiro KJB, Sousa RRM, de Araújo FO, Brito RA, Barbosa JCP, Alves C Jr. Industrial application of AISI 4340 steels treated in cathodic cage plasma nitriding technique. *Mater Sci Eng A*. 2008;479(1-2):142-7. <http://dx.doi.org/10.1016/j.msea.2007.06.033>.
25. Edenhofer B. Physical and metallurgical aspects of ionnitriding. *Heat Treatment of Metals*. 1974;1:23-8.
26. Jindal PC. Ion nitriding of steels. *J Vac Sci Technol*. 1998;15(2):313-7. <http://dx.doi.org/10.1116/1.569579>.
27. Brading HJ, Morton PH, Bell T, Earwaker LG. Plasma nitriding with nitrogen, hydrogen, and argon gas mixtures: structure and composition of coatings on titanium. *Surf Eng*. 1992;8(3):206-12. <http://dx.doi.org/10.1179/sur.1992.8.3.206>.
28. Figueroa CA, Weber S, Czerwicz T, Alvarez F. Oxygen, hydrogen, and deuterium effects on plasma nitriding of metal alloys. *Scr Mater*. 2006;54(7):1335-8. <http://dx.doi.org/10.1016/j.scriptamat.2005.12.013>.
29. Norsuzila Ya'acob M, Abdullah M, Ismail M. Medina TL, Talarico IA, Casas TC, et al. Plasma nitriding of titanium alloys. *Intech*. 1989;32:137-44.
30. Chen KC, Jaung GJ. D.c. diode ion nitriding behavior of titanium and Ti-6Al-4V. *Thin Solid Films*. 1997;303(1-2):226-31. [http://dx.doi.org/10.1016/S0040-6090\(97\)00075-8](http://dx.doi.org/10.1016/S0040-6090(97)00075-8).
31. Vitoriano JDO, Pessoa RS, Mendes AA Fo, Amorim JD Fo, Alves-Junior C. Effect of OH species in the oxynitride titanium formation during plasma-assisted thermochemical treatment. *Surf Coat Tech*. 2022;430:127990. <http://dx.doi.org/10.1016/j.surfcoat.2021.127990>.
32. Saoula N, Madaoui N, Tadjine R, Erasmus RM, Shrivastava S, Comins JD. Influence of substrate bias on the structure and properties of TiCN films deposited by radio-frequency magnetron sputtering. *Thin Solid Films*. 2016;616:521-9. <http://dx.doi.org/10.1016/j.tsf.2016.08.047>.
33. Biesinger MC, Lau LWM, Gerson AR, Smart RSC. Resolving surface chemical states in XPS analysis of first row transition metals, oxides and hydroxides: Sc, Ti, V, Cu and Zn. *Appl Surf Sci*. 2010;257(3):887-98. <http://dx.doi.org/10.1016/j.apsusc.2010.07.086>.
34. Schneider J, Matsuoka M, Takeuchi M, Zhang J, Horiuchi Y, Anpo M, et al. Understanding TiO₂ photocatalysis: mechanisms and materials. *Chem Rev*. 2014;114(19):9919-86. <http://dx.doi.org/10.1021/cr5001892>.
35. Ataíde ARP, Alves C Jr, Hajek V, Leite JP. Effects during plasma nitriding of shaped materials of different sizes. *Surf Coat Tech*. 2003;167(1):52-8. [http://dx.doi.org/10.1016/S0257-8972\(02\)00887-3](http://dx.doi.org/10.1016/S0257-8972(02)00887-3).
36. Skowroński AJ, Antończak AJ, Trzcinski M, Łazarek Ł, Hiller T, Bukaluk A, et al. Optical properties of laser induced oxynitride films on titanium. *Appl Surf Sci*. 2014;304:107-14. <http://dx.doi.org/10.1016/j.apsusc.2014.01.047>.
37. Pohrelyuk I, Morgiel J, Tkachuk O, Szymkiewicz K. Effect of temperature on gas oxynitriding of Ti-6Al-4V alloy. *Surf Coat Tech*. 2019;360:103-9. <http://dx.doi.org/10.1016/j.surfcoat.2019.01.015>.
38. Lebeda M, Vlčák P, Drahokoupil J. Influence of nitrogen interstitials in α -titanium and nitrogen vacancies in δ -titanium nitride on lattice parameters and bulk modulus - computational study. *Comput Mater Sci*. 2022;211:111509. <http://dx.doi.org/10.1016/j.commatsci.2022.111509>.
39. Gray GT 3rd, Lawson AC. Influence of interstitial oxygen on the lattice parameters of solution-treated and aged Ti-8.6 wt% Al alloys. *Proc MRS*. 1989;166:261-6. <http://dx.doi.org/10.1557/PROC-166-261>.
40. Kværndrup FB, Küctükylidiz ÖC, Winther G, Somers MAJ, Christiansen TL. Extreme hardening of titanium with colossal interstitial contents of nitrogen and oxygen. *Mater Sci Eng A*. 2021;813:141033. <http://dx.doi.org/10.1016/j.msea.2021.141033>.
41. Conrad H. Effect of interstitial solutes on the strength and ductility of titanium. *Prog Mater Sci*. 1981;26(2-4):123-403. [http://dx.doi.org/10.1016/0079-6425\(81\)90001-3](http://dx.doi.org/10.1016/0079-6425(81)90001-3).
42. Scotti L, Mottura A. Interstitial diffusion of O, N, and C in α -Ti from first-principles: analytical model and kinetic Monte Carlo simulations. *J Chem Phys*. 2016;144(8):084701. <http://dx.doi.org/10.1063/1.4942030>.
43. Saoula N, Djerourou S, Yahiaoui K, Henda K, Kesri R, Erasmus RM, et al. Study of the deposition of Ti/TiN multilayers by magnetron sputtering. *Surf Interface Anal*. 2010;42(6-7):1176-9. <http://dx.doi.org/10.1002/sia.3299>.
44. Cheng YH, Tay BK, Lau SP, Kupfer H, Richter F. Substrate bias dependence of Raman spectra for TiN films deposited by filtered cathodic vacuum arc. *J Appl Phys*. 2002;92(4):1845-9. <http://dx.doi.org/10.1063/1.1491588>.
45. Stoehr M, Shin CS, Petrov I, Greene JE. Raman scattering from TiN_x ($0.67 \leq x \leq 1.00$) single crystals grown on MgO(001). *J Appl Phys*. 2011;110(8):1-4. <http://dx.doi.org/10.1063/1.3651381>.
46. Vasconcellos MAZ, Hinrichs R, Javorsky CS, Giuriatti G, Borges da Costa JAT. Micro-Raman characterization of plasma nitrided Ti6Al4V-ELI. *Surf Coat Tech*. 2007;202(2):275-9. <http://dx.doi.org/10.1016/j.surfcoat.2007.05.038>.
47. Souza GB, da Silva BA, Steudel G, Gonsalves SH, Foerster CE, Lepienski CM. Structural and tribo-mechanical characterization of nitrogen plasma treated titanium for bone implants. *Surf Coat Tech*. 2014;256:30-6. <http://dx.doi.org/10.1016/j.surfcoat.2013.12.009>.
48. Constable CP, Yarwood J, Münz W-D. Raman microscopic studies of PVD hard coatings. *Surf Coat Tech*. 1999;116-119:155-9. [http://dx.doi.org/10.1016/S0257-8972\(99\)00072-9](http://dx.doi.org/10.1016/S0257-8972(99)00072-9).
49. Challagulla S, Tarafder K, Ganesan R, Roy S. Structure sensitive photocatalytic reduction of nitroarenes over TiO₂. *Sci Rep*. 2017;7(1):1-10. <http://dx.doi.org/10.1038/s41598-017-08599-2>.
50. Ismail IM, Abdallah B, Abou-Kharroub M, Mrad O. XPS and RBS investigation of TiN xO y films prepared by vacuum arc discharge. *Nucl Instrum Methods Phys Res B*. 2012;271:102-6. <http://dx.doi.org/10.1016/j.nimb.2011.11.010>.
51. Kuznetsov MV, Zhuravlev JF, Gubanov VA. XPS analysis of adsorption of oxygen molecules on the surface of Ti and TiN_x films in vacuum. *J Electron Spectrosc Relat Phenom*. 1992;58(3):169-76. [http://dx.doi.org/10.1016/0368-2048\(92\)80016-2](http://dx.doi.org/10.1016/0368-2048(92)80016-2).
52. Zhang M, Lin G, Dong C, Kim KH. Mechanical and optical properties of composite TiO_xN_y films prepared by pulsed bias

- arc ion plating. *Curr Appl Phys.* 2009;9(3):S174-8. <http://dx.doi.org/10.1016/j.cap.2009.01.034>.
53. Saha NC, Tompkins HG. Titanium nitride oxidation chemistry: an x-ray photoelectron spectroscopy study. *J Appl Phys.* 1992;72(7):3072-9. <http://dx.doi.org/10.1063/1.351465>.
54. Wan L, Li JF, Feng JY, Sun W, Mao ZQ. Improved optical response and photocatalysis for N-doped titanium oxide (TiO₂) films prepared by oxidation of TiN. *Appl Surf Sci.* 2007;253(10):4764-7. <http://dx.doi.org/10.1016/j.apsusc.2006.10.047>.